Effects of void size, density, and arrangement on deflagration and detonation sensitivity of a reactive empirical bond order high explosive

S. Davis Herring,[1,2,*] Timothy C. Germann,[1,†] and Niels Grønbech-Jensen[2,‡]
[1]*Theoretical Division, Los Alamos National Laboratory, Los Alamos, New Mexico 87545, USA*
[2]*Department of Applied Science, University of California–Davis, Davis, California 95616, USA*
(Received 8 April 2010; published 13 December 2010)

The shock response of two-dimensional model high explosive crystals with various arrangements of circular voids is explored. We simulate a piston impact using molecular-dynamics simulations with a reactive empirical bond order model potential for a submicron, subnanosecond exothermic reaction in a diatomic molecular solid. Voids of radius 10 nm reduce the minimum initiating velocity by a factor of 4; a single 2.5 nm void (per periodic image) reduces the minimum velocity for detonation by 10% and the exponent of the induction time's pressure dependence by about 4. In square lattices of voids all of one size, reducing that size or increasing the porosity while holding the other parameter fixed causes the hotspots to consume the material more quickly and detonation to occur sooner and at lower piston velocities. The early time behavior is seen to follow a very simple ignition and growth model. The hotspots collectively develop a broad pressure wave (a sonic, diffuse deflagration front) that, upon merging with the lead shock, transforms it into a detonation. The reaction yields produced by triangular lattices are not significantly different. With random void arrangements, the mean time to detonation is 15.5% larger than with the square lattice; the standard deviation of detonation delays is just 5.1%.

DOI: 10.1103/PhysRevB.82.214108 PACS number(s): 62.50.Ef, 47.40.Nm, 82.40.Fp

I. INTRODUCTION

Microscopic defects in solid high explosives can have dramatic effects on the sensitivity of the bulk material to initiation by shock waves.[1,2] When a shock that is insufficiently strong to ignite the material directly encounters a defect, reflection and refraction redirect its energy. Where the energy density is reduced, little changes; the shock was already inert. However, a local, temporary increase in energy density may drive exothermic chemical reactions; the resulting hotspot will not generally cause detonation directly, but will increase the pressure behind the shock and thus its strength. As the shock increases in strength, more energy is available for focusing and less focusing is needed to initiate further reactions. The positive feedback that results is the principal driver of the transition from shock to detonation in heterogeneous explosives.[3] The details of the defect feedback process remain poorly understood,[3] and so practical questions like "to what extent would a population of voids (with some distributions in space and size) reduce the critical velocity of this explosive?" go unanswered.

Spherical voids are an often studied, common defect in cast and formed explosives.[1,3–5] When a sufficiently strong shock wave encounters a void, the leading surface is ejected into the void, and the resulting gas is compressed as the void collapses; jetting may also occur.[1,3,5] The shock's energy is focused onto the downstream pole of the void. If the void is large enough and the shock strong enough, chemical reactions result. This process is illustrated in Fig. 1.

Several attempts to identify the atomistic mechanism of chemical initiation in collapsing voids have been made using molecular-dynamics (MD) simulations.[6] Mintmire *et al.*[7] determined that energy was efficiently transferred into the molecular vibrational modes of a nonreactive diatomic molecular solid only when the collapse of the void was turbulent and involved the disintegration of its walls; such vibrational excitation is thought to be a necessary precursor to chemical reaction. White *et al.*[8] found that randomly placed circular voids significantly affected the response of ozone crystals under shock loading. Germann *et al.*[9] observed that reactions occurred some time after the ejected molecules collided with the downstream wall (and, with a periodic array of voids, could lead to detonation) and that the reduction in critical shock strength for ignition depended on the orientation as well as the size of elliptical voids. In particular, sensitivity was observed to increase with the width of a planar gap, suggesting that heating via recompression of the ejected gas was important for initiation. Holian *et al.*[10] extended the planar gap analysis with a Lennard-Jones potential and derived an expression for the temperature increase due to recompression.

Hatano[11] considered the nonequilibrium mechanics of the ejected material in cuboidal voids and observed that the fre-

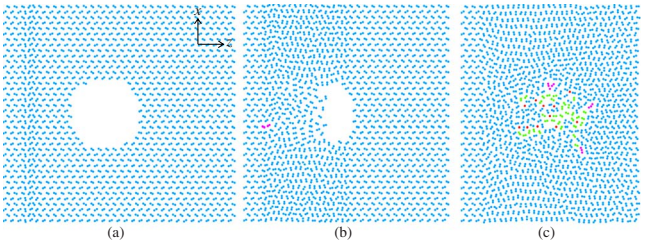

FIG. 1. (Color online) Snapshots from a 124 Å × 135 Å, 2372-atom low-velocity simulation with $r=20$ Å and $u_p \approx 3$ km/s. Undisturbed material at left is the piston; blue (medium gray), green (light), red (darkest), and purple (dark) atoms are reactants, products, radicals, and clusters, respectively (defined in Sec. II C). (a) Just after impact. (b) 200 fs before the void finishes collapsing. (c) End of the simulation; shock has reached the free surface 1.17 ps after impact.

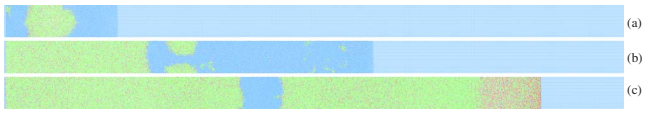

FIG. 2. (Color online) Snapshots of the forward ~40% of a 204 Å×10 013 Å, 313 086–atom high-velocity simulation with r=50 Å and $u_p \approx 4$ km/s; colors as in Fig. 1. (a) The periodic images of the hotspot have merged. (b) Reactions develop between the deflagration and the shock front. (c) Detonation has commenced, separated from the original deflagration; the zone of increased dissociation near the shock corresponds to the overdriving in Fig. 8.

quency of energetic molecular collisions reached a maximum after temperature did and could vary independently of that maximum. Shi and Brenner[12] considered infinite rectangular voids in N_8 cubane crystals and observed reactions following almost immediately after the initial downstream jet impact, with individual molecular collisions at the impact point leading directly to dissociation. Turbulent destruction of the void walls and focusing of the ejecta by the walls were observed to increase sensitivity in that system but recompression after the jet impact (or in the absence of any jet) was not.

Experimental, theoretical, and numerical studies have sought to explain the sensitivity enhancement caused by voids and inert inclusions (which produce effects similar to those of voids by reflecting portions of the shock that may create hotspots where they collide). Bourne and Field[13] reported results from shocked two-dimensional samples of gelatin or an emulsion explosive that had large cylindrical voids introduced. They observed that voids could shield their downstream neighbors from the lead shock but that they could also effect the collapse of their neighbors by emitting shock waves when they collapsed. Dattelbaum *et al.*[14] shocked samples of nitromethane with randomly embedded glass beads or microballoons, observing that their presence decreased the run distance to detonation and the pressure dependence of that distance. The balloons were found to have a greater effect than the beads and small beads were in turn more effective than large beads.

Medvedev *et al.*[15] conducted a theoretical analysis of emulsion explosives with microballoons that explained changes in detonation velocity with microballoon concentration via an ignition and growth model with a constant mass burn rate per hotspot. Bourne and Milne[16] experimentally and computationally considered a hexagonal lattice of cylindrical voids in an emulsion explosive or nitromethane and observed that the reactions at the hotspots accelerated the shock relative to a comparison with water.

To better understand the output of void-based hotspots (as a function of void size and input shock strength) and their ability to precipitate detonation, we use MD simulations of supported shocks in an assortment of two-dimensional samples with circular voids. We first consider single voids (per periodic image): with high enough shock strengths, feedback can develop among scattered reactions in the shocked material and produce a detonation, as depicted in Fig. 2. We also consider structured and unstructured arrangements of voids.

Two-dimensional simulations have significant limitations, of course: the available geometries (for systems, molecules, and collisions) are much restricted, and processes such as diffusion happen at very different speeds. However, the restrictions placed by computer resources on three-dimensional studies may be just as damaging: while single simulations are feasible, systematic parameter studies (including multiple voids) that identify mechanisms and quantify statistical effects are yet not. Hopefully, the results of this study will improve understanding of real systems and inspire the selection of the most helpful more realistic simulations.

II. METHOD

A. Approach

We simulate piston impacts on a number of samples with one or more equal-sized circular voids either randomly placed or in a regular square or triangular lattice. Single voids are placed near the piston; voids in a lattice are evenly spaced along the sample. With the single voids, we perform two separate investigations in different velocity regimes to study the transitions, as radius and/or velocity increase, from no reactions at all to slow deflagration and then to a detonation wave.

We parametrize the possible lattices by their symmetry, the total porosity p (proportion of molecules removed from the perfect crystal), and the radius r of each void. The spacing between voids in the square lattice is then

$$\delta \equiv r\sqrt{\pi/p}. \tag{1}$$

The principal goal is to determine which of these parameters have a significant effect on the sensitivity of the explosive, as measured by the time t_D from piston impact to detonation transition. We also look for nonadditive contributions from the arrangement of voids (rather than their simple number density) and explore the mechanism of the development of detonation.

1. Single voids

Low-strength shocks may collapse a void without producing any chemical reactions. We simulate low-velocity pistons impacting samples with single voids of various radii; Fig. 1 is taken from one such simulation. Each simulation is run until any product molecules are detected (as defined in Sec. II C) or until the shock reaches the free end of the material (by which time the void collapse is finished). Several initial conditions with the same void radius and piston velocity but varied random thermal velocities are considered and the proportion of them in which products appear is taken as the probability of initiation. Very small voids (and the special case of zero void size) are excluded from this study because spontaneous reactions would compete with those triggered by the void and introduce a dependence on the size of the sample.

At higher impact velocities, the hotspot always reacts but may produce a detonation wave only much later if at all. It is difficult to establish with a finite sample that a detonation would never develop from an observed deflagration but the

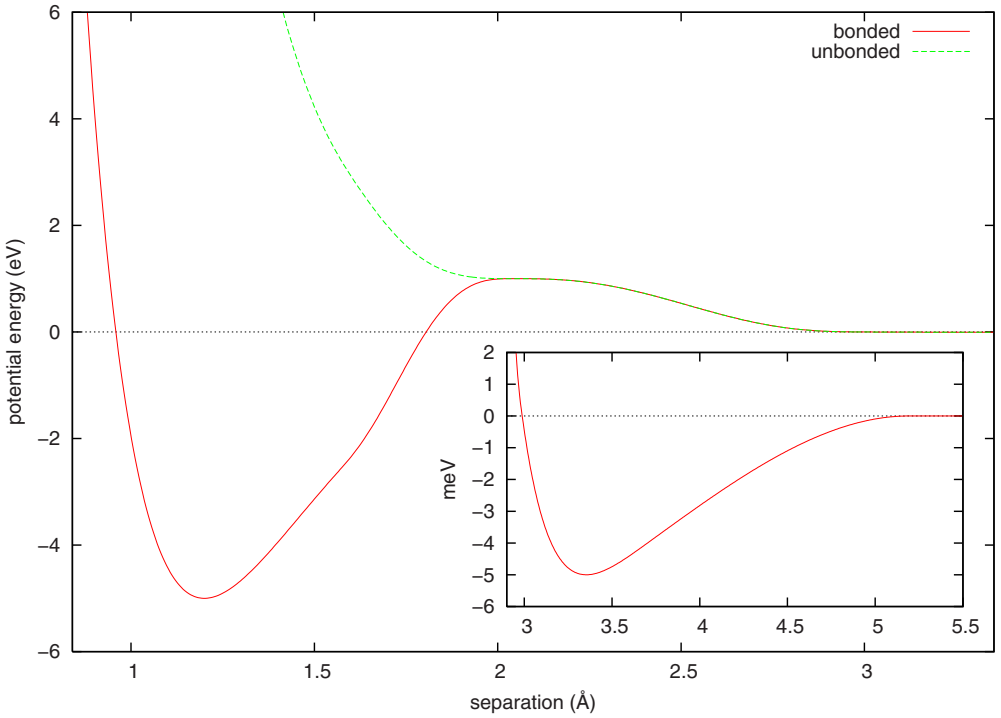

FIG. 3. (Color online) The ModelIV potential-energy functions for bound and unbound pairs of similar atoms. For dissimilar atoms, the covalent well is shallower, but otherwise little differs. The van der Waals minimum is shown in the inset.

progress of the deflagration at moderate velocities and the promptness of the detonation at high velocities may be used to bracket the critical velocity. The high-velocity piston impact simulations are similar to those in the low-velocity study: they involve various void radii and start from several thermally random initial conditions for each case. Figure 2 is taken from one such simulation in which the sample detonated.

The stochastic initiation process is studied in samples having voids of radius 1–10 nm with piston velocities of up to 3.5 km/s. The high-velocity study of the transition to detonation involves samples having voids of radius 1, 2.5, or 5 nm as well as the perfect-crystal case ($r=0$). There, the pistons have velocities of $u_p=2.95–4.90$ km/s and produce pressures of 10.8–20.9 N/m. Such two-dimensional pressures are difficult to interpret physically but following Robertson *et al.*[17] we may suppose that 1 N/m$\approx$2.5 GPa.

2. Multiple voids

We consider 94 square lattices: 27 with an integer number n of voids and 67 with n allowed to merely approximate an integer (so the last void's distance to the end of the sample differs slightly from the first's to the piston). For brevity, we will term these two cases S_1 and S_2, respectively. The extent of these simulations in the periodic x direction is δ.

In Case S_1, each combination of $p\in\{1.0,1.778,2.25\}$% and $r\in\{3,4,6\}$ nm is considered, with $Z=1.28$ μm chosen so that $n\equiv Z/\delta$ is always an integer ($n\in[12,36]$), and each choice is simulated at each piston velocity $u_p\in\{1.96,2.95,3.93\}$ km/s; 694 776–2 070 048 atoms are simulated. In Case S_2, $Z=845$ nm and $u_p=2.95$ km/s are fixed, and the 67 p-r pairs from $\{1.0,1.1,\ldots,2.0\}$% $\times\{15,16,\ldots,59\}$ Å that yield an n within 0.075 of an integer are simulated ($n\in[8,42]$, 260 736–1 341 296 atoms). The fixed velocity and loosened constraint on n allow this study to explore the p-r space more effectively.

In an ancillary study called Case T, rectangular and triangular lattices of $n=10$ voids are each simulated 27 times with a fixed $u_p=1.96$ km/s and every combination of $p\in\{1.0,1.5,2.0\}$%, $r\in\{3,4,5\}$ nm, and $Z\in\{416,521,627\}$ nm. Here the void spacings are $\delta_z=Z/n$ and $\delta_x=\pi r^2/p\delta_z=n\pi r^2/pZ$; 214 060–1 206 248 atoms are simulated.

In the random case, a fixed sample size of 201 nm $\times$1015 nm is used with three different (p,r,u_p) triples taken from the Case S_1 lattices (but with more voids because of the increased sample area): Case R_1 with (1%, 6 nm, 1.96 km/s) and $n=18$, Case R_2 with (2.25%, 6 nm, 1.96 km/s) and $n=40$, and Case R_3 with (2.25%, 4 nm, 2.95 km/s) and $n=90$. For each set of parameters, ten simulations are run with different random arrangements of voids chosen by the simple rejection method such that all void centers are at least $2r$ away from either surface of the sample and at least $4r$ away from each other. This largest case involves $\sim$3.1 million atoms.

B. Model

The reactive empirical bond order (REBO) "*AB*" potential (originally developed in Refs. 6, 17, and 18) describes an exothermic $2AB\rightarrow A_2+B_2$ reaction in a diatomic molecular solid and exhibits typical detonation properties but with a submicron, subnanosecond reaction zone that is amenable to MD space and time scales. With this potential a *bond order* is calculated for each pair of atoms that represents the strength of a covalent bond between them. The bond order, which is the only many-body component of the potential, is 1 for a pair of atoms in isolation, but continuously varies to near 0 for two atoms with several other neighbors at compa-

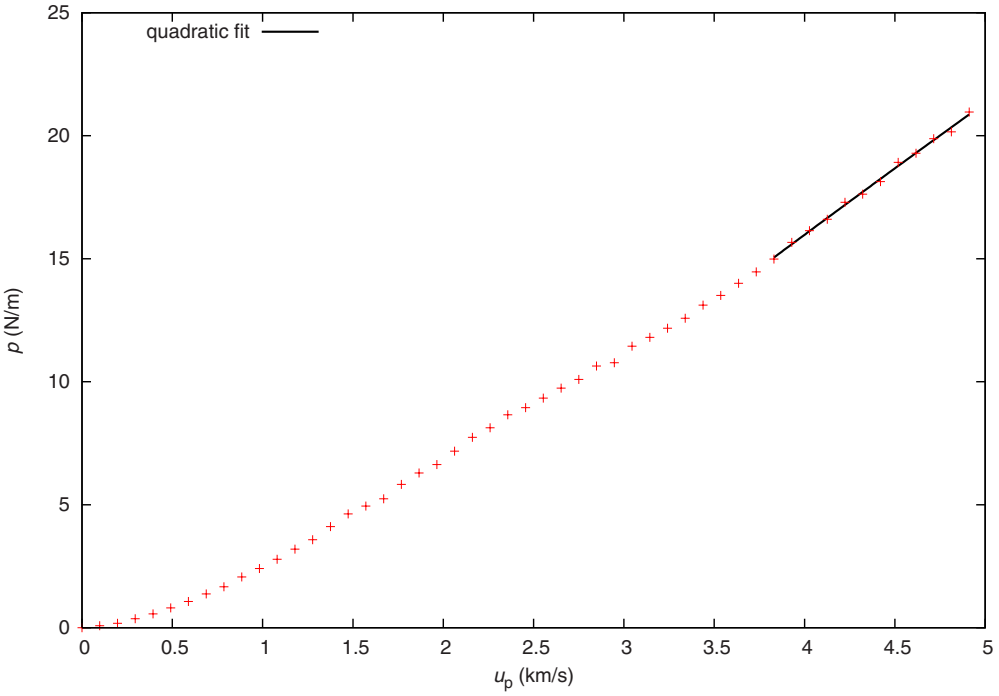

FIG. 4. (Color online) Hugoniot for the unreacted material for piston velocities through the largest used in the high-velocity study. The line is a smoothing quadratic fit through the data points in its interval.

rable or smaller separations. The simplicity of the chemistry and of the potential allows routine multimillion-atom simulations that encompass the entire initiation process.

Heim *et al.*[19] modified it to give a more molecular (and less plasmalike) Chapman-Jouguet state and an increased activation energy of ~2 eV. We utilize the SPaSM (scalable parallel short-range molecular dynamics) code[20] and that modified REBO potential (ModelIV). Figure 3 illustrates the potential for the bond orders of 0 and 1. A standard leapfrog-Verlet integrator is used with a fixed time step of 0.509 fs in the NVE (constant number, volume, and energy) ensemble.

Each two-dimensional sample is a rectangle of herringbone crystal with two *AB* molecules in each 6.19 Å $\times$4.21 Å unit cell, the zero-temperature, zero-pressure ($T=P=0$) minimum-energy configuration. The shock propagates in the $+z$ direction; the samples are periodic in the transverse x direction. Each circular void is created by removing all dimers whose midpoints lie within a circle of a given radius [see Fig. 1(a)]. In the low-velocity cases, the sample is made large enough to prevent interaction between the periodic images of the void until the collapse is finished and the material has or has not reacted. Depending on the size of the void, 672–49 700 atoms are simulated. The high-velocity samples are 1 μm (2381 unit cells) long and two void diameters wide (or 10 nm in the case of no void) with the void center four diameters from the piston face; they include 66 622–313 086 atoms.

Three layers of unit cells at the $-z$ end are frozen to serve as a piston (of infinite mass), and the rest is assigned a tiny but finite temperature (low velocity: 11.6 mK, high velocity: 1.00 mK) and a bulk velocity $v_z=-u_p$ directed into the piston. The temperature is made very small to avoid thermal expansion from the $T=P=0$ state, but kept nonzero to avoid spurious effects from mathematically perfect crystals and to allow multiple thermal initial conditions; the rms atomic displacement it causes is 2.1 pm. (Hugoniot simulations performed at larger temperatures did not produce significantly different shock speeds and all other effects happen at the much higher temperature created by the shock.)

To reduce the correlation between the different histories in the single-void studies, the initial thermal velocities are allowed to thermalize for 1 ps (5 ps for the low-velocity study) before the bulk velocity is applied. Each simulation is run until the shock (whether reacting or not) reaches the free end of the sample; the traversal time of the shock (assuming that it does not accelerate) is $t_t=Z/u_s(u_p)$, where $u_s(u_p)$ is the shock velocity Hugoniot. It is broadly similar throughout the simulations, so the determination of whether or not a detonation occurs is meaningfully consistent. In particular, in each of the principal studies the sample length Z is held fixed so that t_t is constant for each u_p.

C. Analysis

We consider a *bond* to exist between any two atoms whose relative velocity is insufficient to separate them. This analysis ignores changes in bond order but considers the outer region of the potential with positive potential energy (see Fig. 3). At regular intervals, the atoms to which each atom is bound are noted. Unbound atoms are called *radicals* and colored red (darkest). Two atoms each bound only to the other are deemed a molecule; heteronuclear *AB* molecules are *reactants* (blue or medium gray) and homonuclear molecules are *products* (green or light). Many of the results derive from a count of such reacted molecules. Atoms bound but not in a stable molecule are termed *clusters* (purple or dark); Fig. 1(c) involves all four possible labels.

To identify in which simulations and at which times detonations develop, we measure the position of the shock wave (whether reacting or not) at intervals of 51 fs (100 time steps) throughout each simulation. The shock positions are obtained by finding the pair of adjacent columns of well-

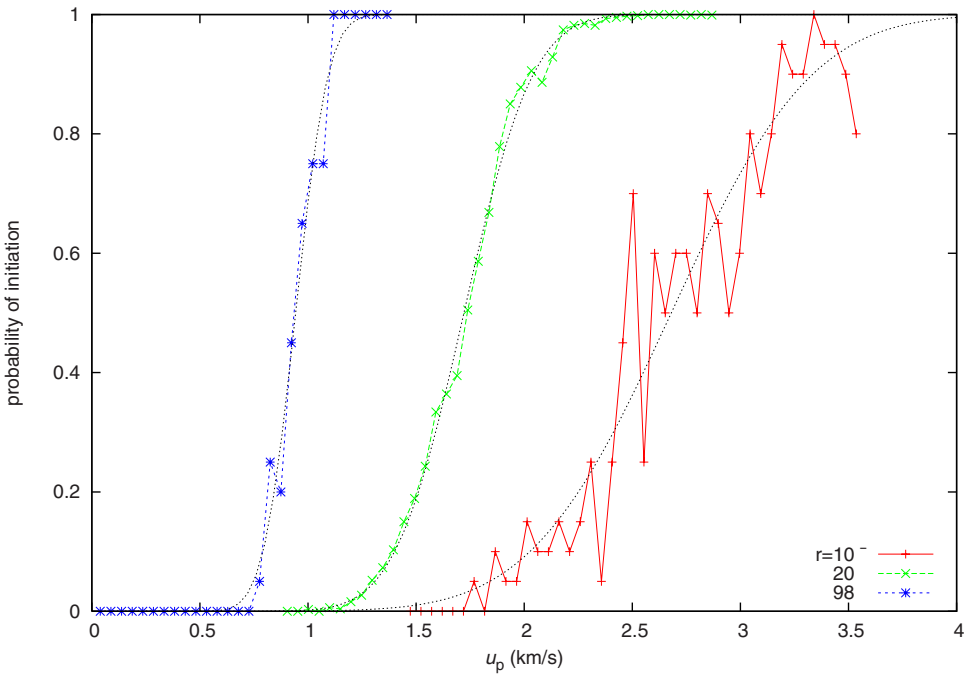

FIG. 5. (Color online) Probabilities of initiation as a function of piston velocity at three selected void radii, each with a sigmoid fit. Larger voids shift the transition to lower velocities and make it sharper. At $r=20$ Å, 1000 simulations were performed per velocity, so the statistical noise is much reduced.

populated computational cells (of thickness $\Delta z \approx 0.53$ nm) with the largest difference in center-of-mass longitudinal velocity $\langle v_z \rangle$. The identified positions are thus only accurate to Δz and are occasionally much too small (when some local fluctuation in the shocked region is misidentified as the shock). Before seeking the detonation transition, the positions are filtered by removing all values smaller than any preceding them.

Detonation transition times are extracted from the filtered shock positions by finding $[(t_1,z_1),(t_2,z_2),(t_3,z_3)]$ triples with z_3-z_2 and z_2-z_1 each $\gtrsim 10$ nm (15 nm with multiple voids) that maximize the weighted second derivative

$$\sqrt{m_2}\frac{m_2-m_1}{t_3-t_1} \quad \left(\text{with } m_i := \frac{z_{i+1}-z_i}{t_{i+1}-t_i}\right), \tag{2}$$

where the additional $\sqrt{m_2}$ slope factor favors the transition to detonation over any sudden acceleration associated with mere deflagration. Maximum scores greater than a manually chosen threshold of 3.9×10^{16} $\mathrm{m}^{3/2}\,\mathrm{s}^{-5/2}$ are taken to indicate detonation transitions. (At low velocities, the void collapse can be mistaken for a transition. These false positives are easily identified by the large gap between them and the true detonations.)

We also determine the shock pressure P associated with a piston velocity u_p from the shock position data. We measure the shock velocities u_s from the beginnings of voidless simulations (to minimize the effects of reactions on the shock positions) and calculate $P=\rho_0 u_s u_p$ (the Hugoniot jump condition with $P_0=0$). For reference, the resulting unreacted Hugoniot is shown in Fig. 4; the pressures used in Sec. III B are smoothed by sampling from a quadratic fit to the highest-velocity data. (The product Hugoniot is presented in Ref. 19.)

III. RESULTS

A. Low-velocity regime: Probability of initiation

Initiation probabilities were derived from at least 20 realizations of each of 1560 radius-velocity pairs (73 553 simulations total). The probabilities obtained for three radii (the largest, the smallest, and an intermediate value with a much larger number of realizations) are given in Fig. 5. At each radius $(10,12,14,\ldots,98$ Å), the critical velocity $u_{p,50}$ (as explored in Ref. 9) and transition sharpness a were determined by scaling and shifting the sigmoid function $P_0(x) := (1+\mathrm{erf}\, x)/2$ in velocity to fit the measured probabilities,

$$P(u_p) \approx \frac{1+\mathrm{erf}\, a(u_p-u_{p,50})}{2}. \tag{3}$$

(Other similar functions [e.g., the logistic function $L(x) := (1+e^{-x})^{-1}$] were considered; $P_0(x)$ was selected because its width-slope product was judged most similar to that in the data.) Figure 5 also contains the sigmoid fits for its three radii.

The parameters in Eq. (3) for all radii are given in Fig. 6. Also shown are fits to the center (the 50% contour) and scale parameters as functions of radius,

$$u_{p,50}(r) \approx \frac{\alpha}{r}+\beta \tag{4}$$

and

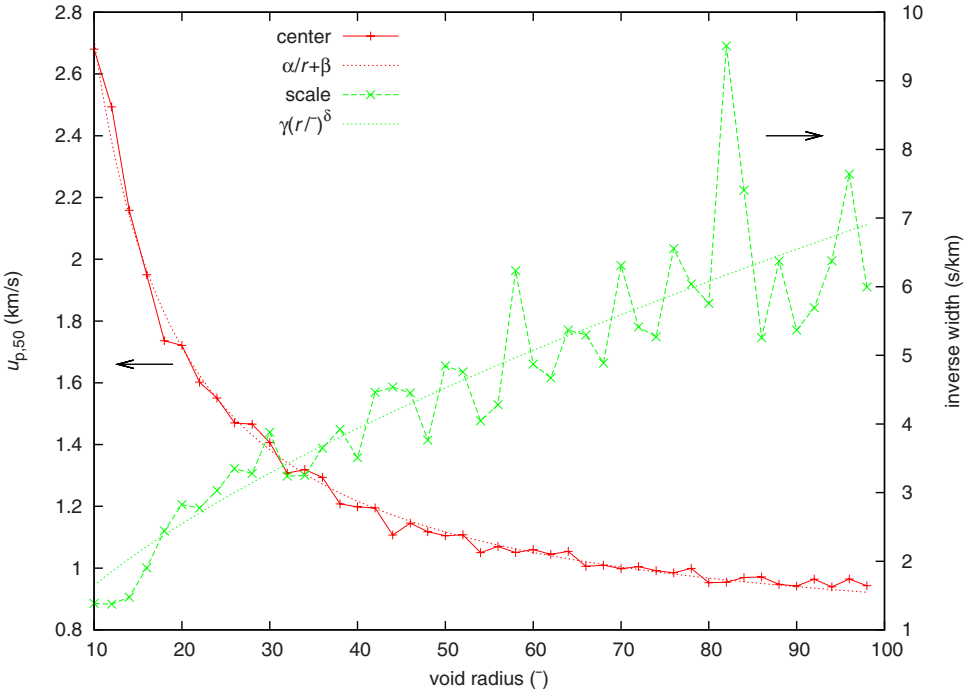

FIG. 6. (Color online) Fit parameters [see Eq. (3)] for the initiation probability as a function of piston velocity at each void radius with fits to them using Eqs. (4) and (5). Larger inverse widths correspond to more sudden transitions from no reactions to guaranteed reactions.

$$a(r) \approx \gamma\left(\frac{r}{\text{Å}}\right)^{\delta}, \tag{5}$$

where $\alpha = 1.99 \times 10^{-6}$ m^2/s, $\beta = 718$ m/s is the asymptotic value for large voids, $\gamma = 3.88 \times 10^{-4}$ s/m, and $\delta = 0.628$. The critical velocity for initiation decreases with radius, as the void focuses more of the shock and creates higher temperatures; at $r = 10$ nm it is a factor of 4 lower than the minimum velocity observed to initiate reactions in a voidless sample. The width (in velocity) of the transition also decreases with increasing void radius, as the hotspot development becomes less dependent on the stochastic behavior of individual molecules. The empirical form Eq. (4) is discussed further in Sec. IV.

B. High-velocity regime: Transition to detonation

Each of 79 radius-velocity pairs was simulated 20 times, each until the shock broke out at the free surface. In each simulation, the maximum number of reacted atoms observed (typically also the final count) was noted. The average count for each r-u_p pair, as a fraction of the total number of atoms, is given in Fig. 7. Even when the reaction consumes the entire sample, the conversion to A_2 and B_2 is not complete;

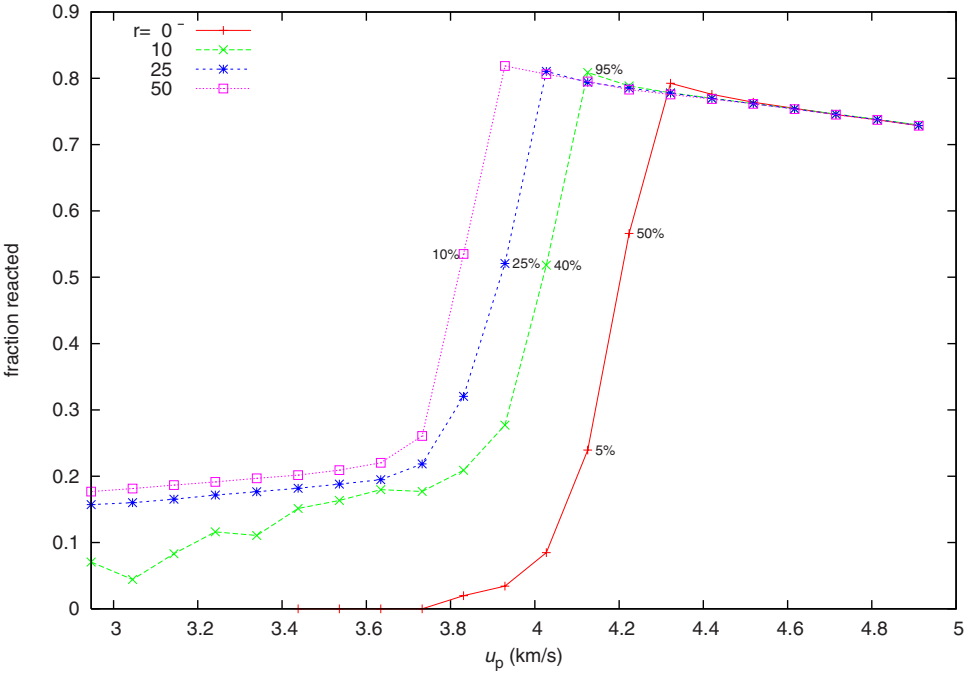

FIG. 7. (Color online) Average maximum extent of reaction at each piston velocity and void radius. Values in the upper plateau (reaction extents >70%) indicate reliable detonation; no detonations occur in most other cases. Percentages of simulations with detonations not 0% or 100% are labeled.

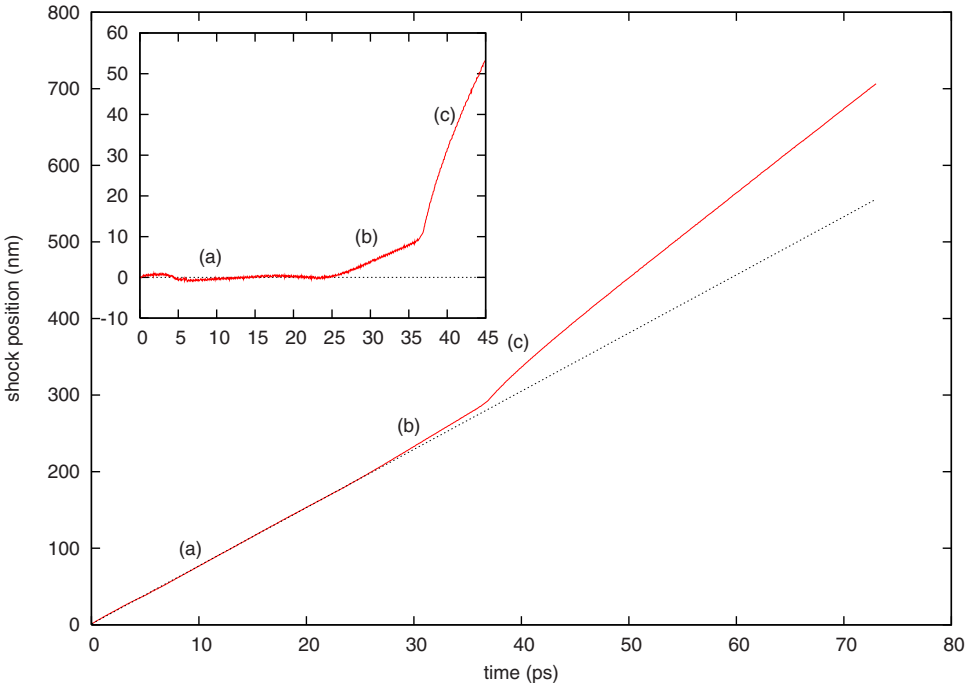

FIG. 8. (Color online) History of the shock position in the simulation from Fig. 2. The times of those snapshots are marked. The detonation transition is clearly visible; the dotted straight line indicates the inert shock's speed. The inset shows the difference between the two.

reaction extents >70% indicate reaction of the entire sample (and thus detonation since the reaction reached the shock front). At velocities above 4.4 km/s, detonation is inevitable regardless of void size (or even presence); the reaction extent decreases slightly as velocity increases further because at higher temperatures the production of radicals rather than products is entropically favored.

At velocities of 3.0–3.6 km/s, the hotspot consistently establishes a growing deflagration in the sample that merges with its periodic images and becomes planar but is left behind by the shock and does not become a detonation. This process produces the consistent reaction extents of approximately 20% that appear for all nonzero void sizes in Fig. 7. The drop-off in the $r=10$ Å data below $u_p=3.4$ km/s is largely due to failure to create a reacting hotspot, rather than due to reacting hotspots quenching. For larger voids, that drop-off moves off below the u_p range of the plot, and the "shoulder" of deflagration widens. The step up to detonation moves more slowly and is of limited utility in identifying a critical velocity because more simulation time (with a larger sample) might allow some of the deflagrations to become detonations. For this transition region, the percentages of simulations that led to detonation (before the shock traversed the 1 μm of sample length) are noted.

The shock positions from a representative simulation that developed a detonation (the same simulation shown in Fig. 2) are shown in Fig. 8 (the Δz-scale roughness is invisibly small). Prior to the transition, reactions developing behind the shock accelerate it; this acceleration occurs even in the samples without voids, where one would expect the shock to accelerate only at transition (when the homogeneous initiation catches up from the piston face). The conditions that inspire a detonation within such small homogeneous samples entail a chemical induction time so short that randomly distributed hotspots appear spontaneously and drive the detonation in the same fashion as in the heterogeneous case.

Temperature profiles at four times during the same simulation are given in Fig. 9. In the first three profiles, the position of the lead shock is evident, and several deflagrations are spreading through the shocked material (separated by unburned regions marked "1" in the figure). The transition to detonation occurred at $z=290$ nm; the steady detonation that develops ("4") has a temperature between that of the deflagration and of the nascent detonation ("3"). The material stagnates against the piston, so the interface between the regions of deflagration and detonation remains nearly stationary. The very short range of heat conduction on this time scale allows that interface to be visible in the temperature profile even at the end of the simulation.

The regions of reduced and increased temperature around the transition ("2" and "3," respectively) illuminate the mechanics of the transition. The material immediately behind the shock shortly before detonation is compressed while inert to the pressure produced by the reactions further upstream. When it reacts, it produces an even higher pressure that accelerates the shock beyond the steady detonation speed. The first detonated material thus reaches an abnormally high temperature ("3"). The rarefactions that reduce the detonation's strength to its steady value also reduce the temperature of the material just behind the transition point ("2").

The minimum transition times for each r-u_p pair (for which any detonations were observed) are given as a function of shock pressure (see Sec. II C) in Fig. 10, along with fits for the power-law dependence normally exhibited for

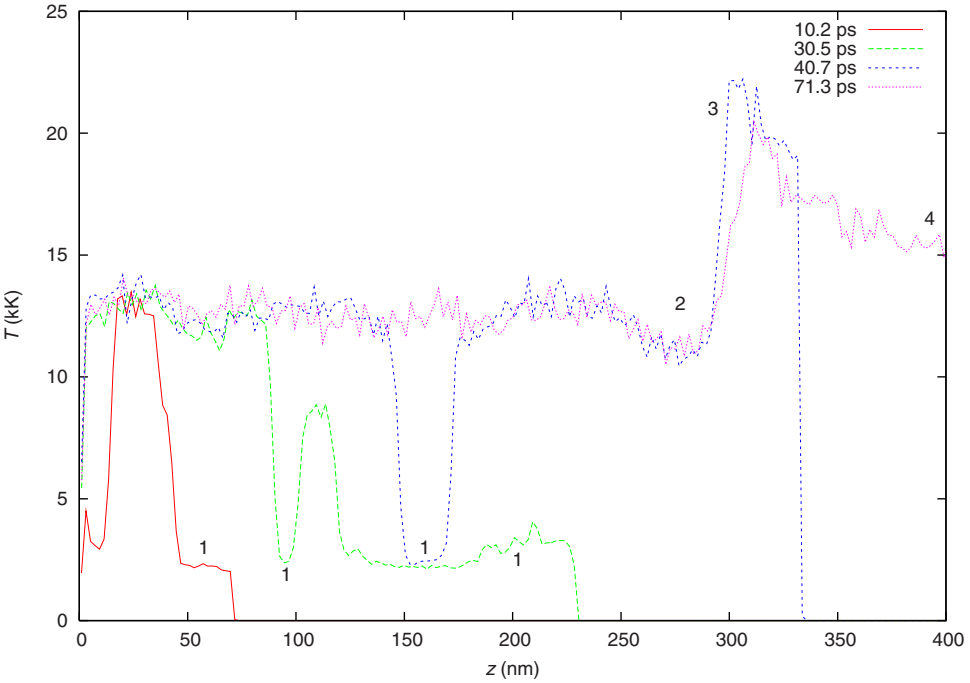

FIG. 9. (Color online) Temperature profiles from the simulation from Fig. 2 over approximately the same region of the simulation. The first three traces correspond to those snapshots; the last is from the end of the simulation and illustrates the stability of the features. Temperatures of 2.5, 12.5, and 15 kK correspond to the inert shock, deflagration in the shocked region, and detonation, respectively. Number labels are referenced in the text.

such Pop plots.[21] For comparison, the medians are also given for those voidless velocities for which a majority of simulations produced detonations; the medians for other void sizes behave similarly, with a nearly constant ratio between the minimum and median times. We see pressure dependences of $P^{-13.77}$ with no void and $P^{-9.95}$ with any size of void, both much larger than the (space-pressure) exponents of −1.6 for PBX-9501 (Ref. 22) and −4.5 for PBX-9502.[23] This discrepancy may arise from the dimensionality of the system and the associated unusual pressure units.

At very high pressures, the void is irrelevant even to the promptness of the detonation, as many reactions are initiated directly upon the piston face. (The largest voids even retard the high-pressure transitions, perhaps due to their greater distance from the piston.) At lower pressures, the presence of a void greatly accelerates the development of a detonation by

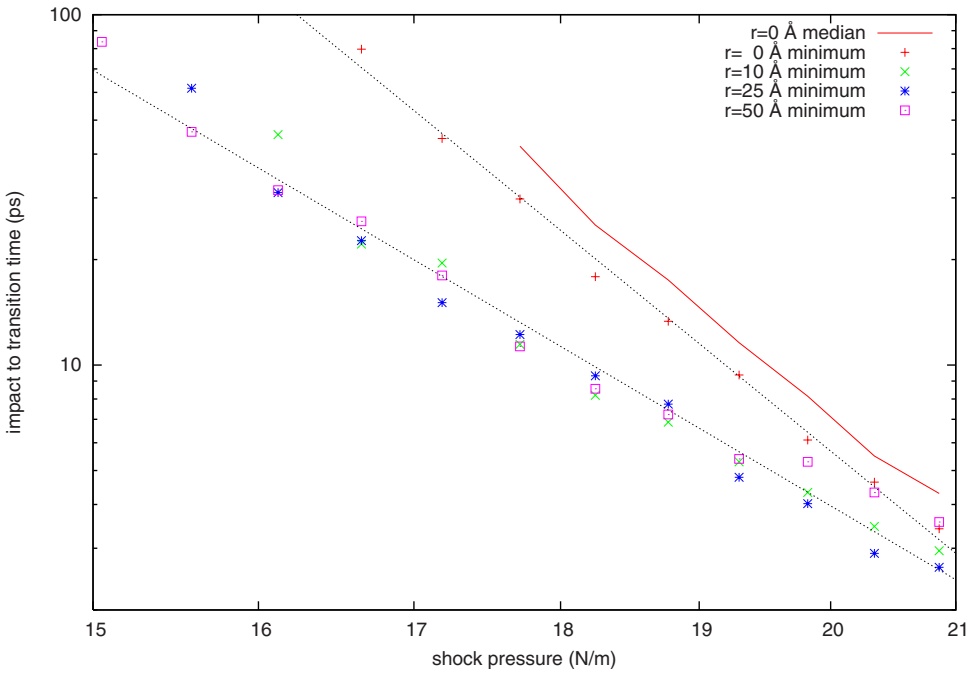

FIG. 10. (Color online) Pop plot of the minimum times to detonation with power-law fits to the no-void data and to all the data with voids. The median times to detonation are also presented for the no-void case for illustration.

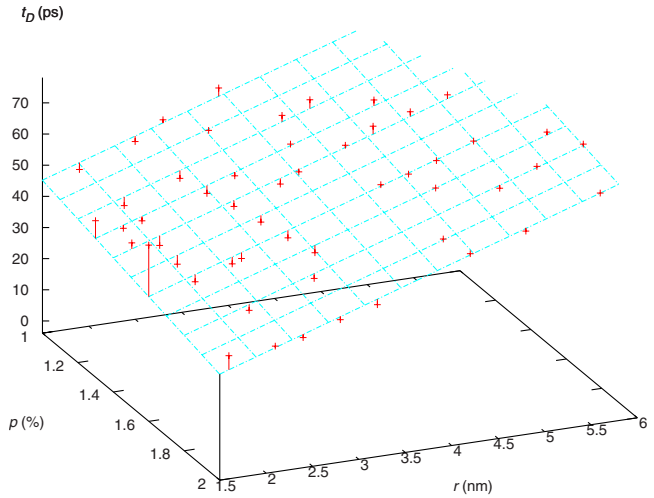

FIG. 11. (Color online) Detonation transition times t_D from Case S_2. The grid shows every p and every fourth r value and is a planar fit to the data, which are shown as crosses connected to it by lines to place them in space and indicate the discrepancies. The upper limit of the plotting region is the length of the longest, nondetonating simulations (78.2 ps).

providing a guaranteed source of significant deflagration but the size of the void seems not to significantly affect the subsequent positive feedback that develops the detonation. However, the transition times for the three nonzero radii separate at low pressures, where the energy available from the hotspot becomes the determining factor in developing a detonation. It happens that this change in the pressure exponent (for each radius) occurs just as the transition times become longer than the simulation and so corresponds precisely to the lower limit of detonations in Fig. 7.

C. Square lattices

The transition times for the 53 (of 67) Case S_2 samples that detonated are shown in Fig. 11. The plane is a fit to the data; its equation is $t_D(p,r)/\mathrm{ps}=9.718r/\mathrm{nm}-1506p+45.67$. The cases that did not detonate before the shock reached the free surface ($t_t \approx 78.2$ ps) would occupy the rear corner of the plot (smallest p and largest r). The proportion of atoms that form product molecules was generally 85% but dropped to 65% in that corner. The half of those 14 simulations closer to the ones which detonated ended with detonation evidently imminent but they are not counted as having detonated since a transition time could not be identified.

At early times, we observe that the extent of reaction closely follows a very simple ignition and growth model. Suppose that a reacting hotspot is a disk that is created with a finite radius r_0 upon collapse of the void and grows at a constant speed v into the surrounding unreacted material until it overlaps its periodic images. If the disk contains a constant areal number density n_a of reacted atoms, the number of reacted atoms as a function of time since initiation has the form

$$N(t) = n_a R(t)^2 = n_a \pi (r_0 + vt)^2. \quad (6)$$

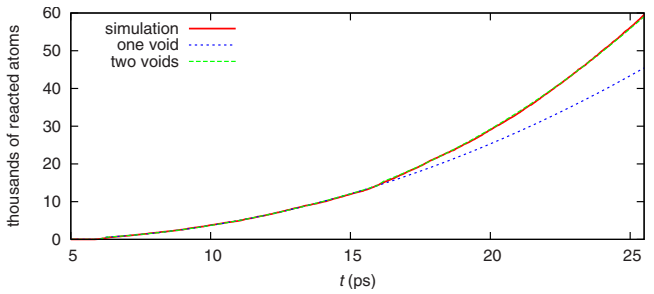

FIG. 12. (Color online) Growth of reaction from the first two voids in a sample with $p=1\%$ and $r=59$ Å. The values from the ignition and growth model applied to the first void and to the first two voids are also shown; the latter curve is almost everywhere indistinguishable from the simulation values.

In Fig. 12 are plotted the counts of reacted atoms from the beginning of the least reactive Case S_2 simulation (before any voids overlap) and the results of fitting one and two copies of $N(t)$ to them, corresponding to the first and then the second periodic line of voids being ignited. The two copies use the same two growth parameters ($r_0\sqrt{n_a}$ and $v\sqrt{n_a}$) and are merely each shifted in time to match the data; the statistical noise from atom counting is invisibly small. Other Case S_2 simulations have similar behavior, but the growth parameters depend in an unknown fashion on r and u_p, so we have no general model for $N(r,u_p,t)$.

Figure 13 shows the temperature distribution history from the other extreme Case S_2 simulation with the smallest (eligible) r at the largest p. Each point in the figure is calculated with respect to the center of mass motion of, and averaged over, a column of computational cells of width $\Delta z \approx 0.53$ nm. We note here the development of a broad pressure wave in the shocked material, visible both as a region of strong advection intersecting the detonation transition and as a temperature increase between the last few hotspots created

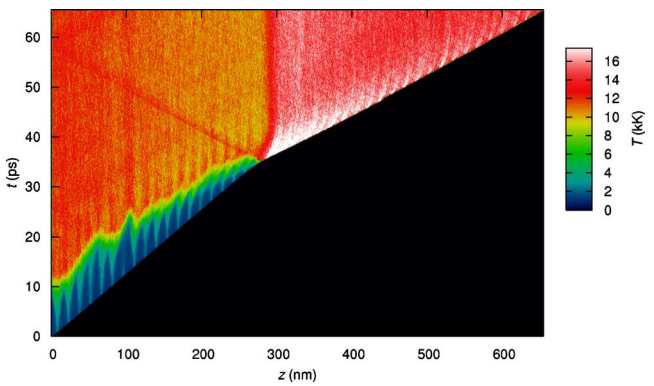

FIG. 13. (Color online) Temperature over space and time in a sample with a square lattice of 42 voids: $p=2\%$, $r=16$ Å, $u_p=2.95$ km/s. Only the region of space occupied by the sample at its final compression is shown. Each spire at the lower left is a hotspot; the very hot region at large z, bounded below by a much faster shock, is the detonation. Note the left-moving shock generated at the transition and the pressure wave (apparent as a temporary strong advection) visible in the shocked material between $z=150$ nm and $z=400$ nm.

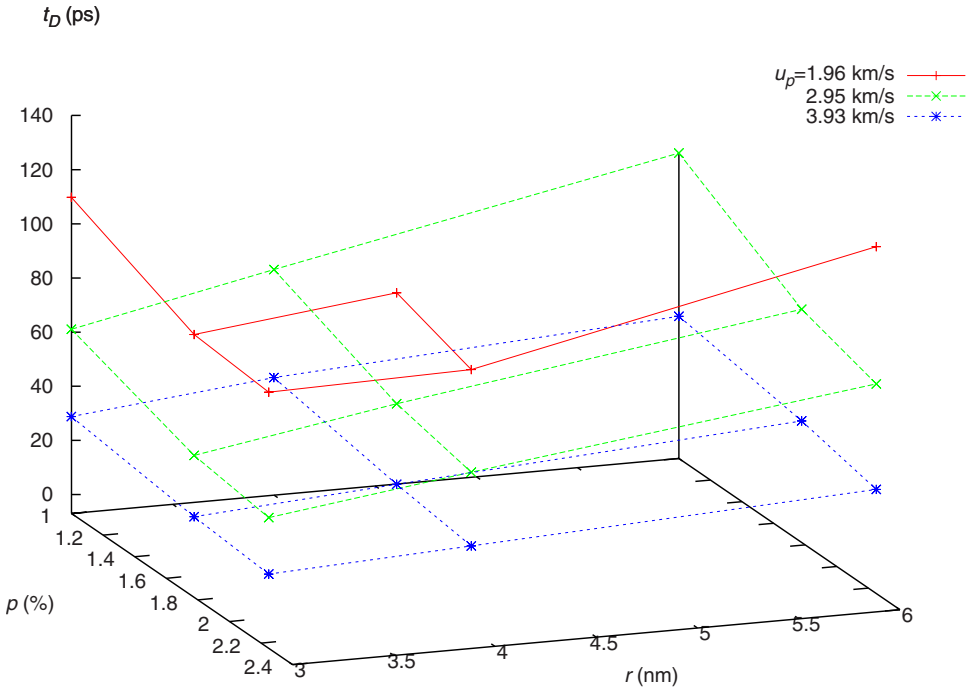

FIG. 14. (Color online) Detonation transition times t_D from Case S_1. The missing points for the smallest u_p indicate failures to detonate.

before the transition. It appears that the pressure waves emitted by the first several hotspots merge and the combined wave strengthens itself by encouraging the deflagration at each hotspot it encounters. When this wave overtakes the lead shock, its particle velocity is approximately equal to u_p=2.95 km/s, so the relative velocity in the collisions at the shock doubles and detonation begins immediately.

All but three of the 27 Case S_1 simulations produced a detonation; those that did not used the lowest u_p and (again) occupied the $-p/+r$ corner of that slice of the parameter space. The transition times for the rest are shown in Fig. 14; they follow the pattern of Case S_2 with the unsurprising addition that $\partial t_D/\partial u_p < 0$. The middle surface has the same u_p as Case S_2 and shows some nonplanarity beyond the range of Fig. 11. With appropriate p and r, we see detonations even at $u_p < 2$ km/s, which is much smaller than any value observed to trigger detonation with merely one periodic rank of voids; the feedback is much strengthened by the subsequent hotspots.

D. Other lattices

In Case T, the rectangular and triangular lattices did not differ significantly: they produced similar reaction yields and no detonations (presumably because they were relatively short; the Case S_1 simulations corresponding to the most reactive case treated here detonated after 87–90 ps). We would expect the triangular case to have a greater reactivity than the rectangular because the overlap between hotspots in adjacent columns is delayed by their offset. The difference is never more than 5% of the area, however, and lasts only until the overlap is complete (about 30% of the reaction phase), so it may be difficult to measure.

For Case R_3, a consistent transition time of t_D =59.3 ps ± 5.1% was observed. The mean is 15.5% larger than the t_D from the corresponding Case S_1 simulation; the small standard deviation suggests that the details of the void arrangement are not significant. Furthermore, examination of one such simulation shows that a tight arrangement of five voids approximately 30% of the way down the sample produces no extra reactions. Later, a triangle of six voids triggers the transition, but spontaneous reactions elsewhere along the shock are also doing so simultaneously, as shown in Fig. 15. None of the other random arrangements detonated. Case R_2 produced yields of 68.0% ± 3.7% (where the second percentage is relative) whereas its Case S_1 counterpart detonated. Case R_1 produced 52.1% ± 6.3% as compared to 70.1% for its counterpart. These differences are between normalized quantities, yet are partially due to the fact that the Case S_1 samples were 26.1% longer.

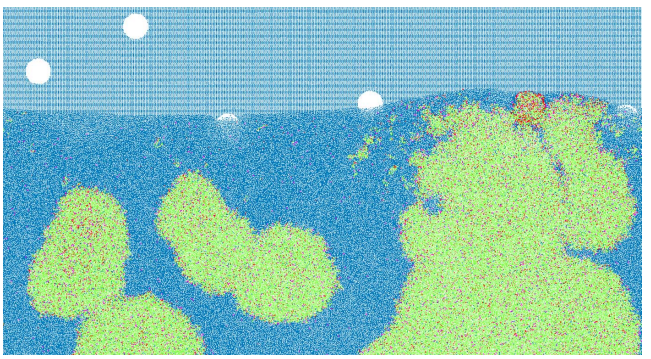

FIG. 15. (Color online) Snapshot from a Case R_3 simulation just as the upward-propagating shock is becoming a detonation. The whole width of the sample but only one ninth of its (original) length is shown; colors as in Fig. 1. The red (dark) disk is a fresh hotspot; note the isolated reactions close to the shock everywhere.

IV. DISCUSSION

We have obtained a simple form [Eq. (4), Fig. 6] for the piston velocity needed to create a reacting hotspot from a void of a given radius in a two-dimensional ModelIV REBO high explosive crystal. In the limit of large voids (with $u_p = \beta$) it appears sufficient to give each dimer just 70 meV of kinetic energy (3.5% of the activation energy). A difference of less than 400 m/s in piston velocity is expected to switch from 10% to 90% chance of ignition for voids with $r > 10$ nm.

Several models were considered for the critical velocity but Eq. (4) was far more successful than the other fits. Given the constant initial density ρ_0, Eq. (4) seems to suggest the existence of a threshold E^* for the kinetic energy missing because of the void. That is, ignition occurs when

$$E := \frac{1}{2}\rho_0 u_p^2 \pi r^2 \geq E^*. \tag{7}$$

That the asymptotic u_p appears nonzero indicates that the effective void collapse mechanism requires a minimum-energy input to function. Holian *et al.*[10] estimate such a minimum from the binding energy of the solid; to adapt their result to a diatomic material, we equate the shock energy per dimer $E_s = \frac{1}{2} m_D u_p^2$ with twice the intermolecular binding energy per dimer, measured as $E_b = 34.7$ meV. (We use $2E_b$ because only half the energy is found in the molecular translational modes that can vaporize the material.) The resulting $u_p^* = 718$ m/s agrees with β to within a surprising 0.08%.

That no additional $u_p > u_p^*$ is needed for large voids attests to the efficacy of the void curvature; while for the planar gap that Holian considers the temperature increase is bounded for large thicknesses, the flow across a circular void of any size is subject to focusing and jetting effects that may strengthen arbitrarily with radius. Germann *et al.*[9] have previously observed such joint effects of curvature and area.

At higher velocities, we have observed a transition from steady deflagration to steady detonation in the range of 4.0 ± 0.4 km/s (an average kinetic energy of 1.1 eV per atom). Its precise, radius-dependent location is nontrivial to establish, but these results suggest the form $u_c(r) \approx (3.8 + 0.34 e^{-r/22\ \text{Å}})$ km/s. As larger samples (and thus longer simulation times) might allow more detonations to finish developing, this expression is probably an overestimate.

The detonation initiation mechanism observed is neither the superdetonation associated with homogeneous explosives[3] nor purely the ignition and growth of (the single rank of) hotspots, although such growth is observed [see Fig. 2(a)]. Rather, the heat and pressure produced by the deflagration outpace it, encourage further reactions throughout the shocked material [see Fig. 2(b)], and strengthen the shock until it ignites the material directly. (The sample width [or distance between periodic images of the void] may affect the feedback; a larger sample provides more possible reaction sites but also more material over which to disperse the void's output.) These results suggest that even isolated nanoscopic features may directly affect bulk material behavior through the positive feedback inherent to energetic materials.

We have also observed the typical power-law dependence of detonation induction time on (two-dimensional) shock pressure, although the exponent seems to change at lower pressures. To our knowledge, such a result has not previously been reported for an MD simulation. It remains to be seen whether such a relationship holds in three-dimensional systems (whose pressures are more meaningful).

It is to be expected that the detonation transition time t_D decreases with an increase in either the porosity p or piston velocity u_p, but that it increases with radius $(\partial t_D / \partial r > 0)$ deserves further consideration. First it should be noted that $(\partial t_D / \partial r)_\delta < 0$: enlarging each of a set of voids without moving them (i.e., keeping the separation δ fixed) does enhance the reactivity. However, when holding p fixed the reduction in number density overwhelms the effect of increasing the void size.

The simple ignition and growth model used earlier provides an explanation. Before any detonation begins, any point in the material is reacted if and only if it is closer to the location of a void collapse than the $R(t)$ associated with that void.[24] Since all voids near a given point will collapse at nearly the same time, what matters is the expected minimum distance $\langle d_{\min} \rangle$ to a void (after shock compression). We expect that $\langle d_{\min} \rangle \propto \delta \propto r$, so the material will react sooner, on average, with small voids—until, of course, the voids become so small that they no longer reliably produce any reactions at all.

A caveat is that if r_0 or v is a strong function of r, the larger average distances from larger voids might be overwhelmed by more vigorous growth of the hotspots created by larger voids. While we do not have a model for $r_0(r, u_p)$ and $v(r, u_p)$, they appear to be weak (perhaps sublinear) functions of r, in which case the conclusion of more reactivity from smaller voids holds. That v is a function of r at all is interesting; we suppose that the r-dependent strength of the reshock emitted when the void collapses and explodes in place may imprint on its surrounds a memory of the void's size.

The model also explains how disorder in the arrangement of voids increases t_D. Whenever, in the random placement of voids, two or more are placed much closer than δ to one another, their hotspots will overlap very quickly and the total burn front area will then be reduced; equivalently, $\langle d_{\min} \rangle$ is larger for a random arrangement than for a lattice (especially a hexagonal one) at the same p and r.

The broad pressure wave created by the lead hotspots seems to be the principal mechanism for the detonation transition in this system. Its development, the identical growth of the first two hotspots, the similarity of the results from rectangular and triangular lattices, the consistency among the results from random void arrangements, and the apparent irrelevance of void clusters all suggest that the development of a detonation is a collective effect that depends on p, r, and the regularity of the void arrangement but not on the details of that arrangement. This collectivity affords a major simplification in predicting the behavior of collections of voids: a model might need only r, p, and σ_δ.

We expect that these general results will apply in three dimensions as well; results with single spherical voids (in preparation) suggest that their individual behavior is qualita-

tively similar to the circular voids considered here. Finally, we note that the function $v(r,u_p)$, since it will likely dominate $r_0(r,u_p)$ and appears to depend on both its arguments but not on time, may prove useful as a measure of the strength or activity of a hotspot that might be incorporated into an analytical reaction rate model. For voids of nonuniform size, it might be sufficient to consider the variation in v in calculating a point's expected burn time.

ACKNOWLEDGMENTS

This report was prepared by Los Alamos National Security under Contract No. DE-AC52-06NA25396 with the U.S. Department of Energy. Funding was provided by the Advanced Simulation and Computing (ASC) program, LANL MDI under Contract No. 75782-001-09, and the Fannie and John Hertz Foundation.

*herring@lanl.gov
†tcg@lanl.gov
‡ngjensen@ucdavis.edu

[1] F. P. Bowden and A. D. Yoffe, *Initiation and Growth of Explosion in Liquids and Solids* (Cambridge University Press, Cambridge, England, 1952).
[2] E. L. Lee and C. M. Tarver, Phys. Fluids **23**, 2362 (1980).
[3] R. Menikoff, in *Shock Compression of Condensed Matter*, AIP Conf. Proc. Vol. 1195, edited by M. Elert, M. D. Furnish, W. W. Anderson, W. G. Proud, and W. T. Buttler (Springer, New York, 2009), pp. 18–25.
[4] *Explosive Effects and Applications*, High Pressure Shock Compression of Condensed Matter, edited by J. A. Zukas and W. P. Walters (Springer, New York, 1998).
[5] C. L. Mader, *Numerical Modeling of Explosives and Propellants* (CRC Press, Cleveland, 1998).
[6] C. T. White, D. R. Swanson, and D. H. Robertson, in *Chemical Dynamics in Extreme Environments*, Advanced Series in Physical Chemistry Vol. 11, edited by R. A. Dressler (World Scientific, Singapore, 2001), Chap. 11.
[7] J. W. Mintmire, D. H. Robertson, and C. T. White, Phys. Rev. B **49**, 14859 (1994).
[8] C. T. White, J. J. C. Barrett, J. W. Mintmire, M. L. Elert, and D. H. Robertson, in *Decomposition, Combustion, and Detonation Chemistry of Energetic Materials* (Materials Research Society, Pittsburgh, USA, 1996), Vol. 418, pp. 277–280.
[9] T. C. Germann, B. L. Holian, P. S. Lomdahl, A. J. Heim, N. Grønbech-Jensen, and J.-B. Maillet, 12th International Symposium on Detonation (Office of Naval Research, Arlington, VA, 2002), pp. 711–717.
[10] B. L. Holian, T. C. Germann, J.-B. Maillet, and C. T. White, Phys. Rev. Lett. **89**, 285501 (2002); **90**, 069902(E) (2003).
[11] T. Hatano, Phys. Rev. Lett. **92**, 015503 (2004).
[12] Y. Shi and D. W. Brenner, J. Phys. Chem. C **112**, 6263 (2008).
[13] N. Bourne and J. Field, in *19th International Congress on High-Speed Photography and Photonics*, edited by B. Garfield and J. Rendell (International Society for Optical Engineering, Bellingham, WA, 1991), Vol. 1358, pp. 1046–1056.
[14] D. M. Dattelbaum, S. A. Sheffield, D. B. Stahl, and A. M. Dattelbaum, Proceedings of the Joint Army-Navy-NASA-Air Force Meeting, 2009 (unpublished).
[15] A. Medvedev, V. Fomin, and A. Reshetnyak, Shock Waves **18**, 107 (2008).
[16] N. K. Bourne and M. A. Milne, Proceedings of the 12th International Detonation Symposium (Office of Naval Research, Arlington, VA, 2002), pp. 213–219.
[17] D. H. Robertson, D. W. Brenner, and C. T. White, Phys. Rev. Lett. **67**, 3132 (1991).
[18] D. W. Brenner, D. H. Robertson, M. L. Elert, and C. T. White, Phys. Rev. Lett. **70**, 2174 (1993); **76**, 2202(E) (1996).
[19] A. J. Heim, N. Grønbech-Jensen, E. M. Kober, J. J. Erpenbeck, and T. C. Germann, Phys. Rev. E **78**, 046709 (2008).
[20] P. S. Lomdahl, P. Tamayo, N. Grønbech-Jensen, and D. M. Beazley, *Proceedings of the Supercomputing Conference* (IEEE Computer Society Press, Los Alamitos, CA, United States, 1993), p. 520.
[21] J. B. Ramsay and A. Popolato, Proceedings of the Fourth International Detonation Symposium (Office of Naval Research, Arlington, VA, 1995), pp. 233–238.
[22] *LASL Explosive Property Data*, Los Alamos Series on Dynamic Material Properties, edited by T. R. Gibbs and A. Popolato (University of California Press, Berkeley, 1980).
[23] B. L. Wescott, D. S. Stewart, and W. C. Davis, J. Appl. Phys. **98**, 053514 (2005).
[24] A. L. Nichols, in *Shock Compression of Condensed Matter*, AIP Conf. Proc. No. 845 (AIP, New York, 2006), p. 465.